
Unfolding recurrence by Green's functions for optimized reservoir computing

Sandra Nestler^{1,2,5}, Christian Keup^{1,5}, David Dahmen¹,
Matthieu Gilson^{1,4}, Holger Rauhut², Moritz Helias^{1,3}

¹Institute of Neuroscience and Medicine (INM-6), Jülich Research Centre, Jülich, Germany

²Mathematics of Information Processing, RWTH Aachen University, Aachen, Germany

³Department of Physics, RWTH Aachen University, Aachen, Germany

⁴Universitat Pompeu Fabra, Barcelona, Spain

⁵RWTH Aachen University, Aachen, Germany

{s.nestler,c.keup,d.dahmen,m.gilson,m.helias}@fz-juelich.de,
rauhut@mathc.rwth-aachen.de

Abstract

Cortical networks are strongly recurrent, and neurons have intrinsic temporal dynamics. This sets them apart from deep feed-forward networks. Despite the tremendous progress in the application of feed-forward networks and their theoretical understanding, it remains unclear how the interplay of recurrence and non-linearities in recurrent cortical networks contributes to their function. The purpose of this work is to present a solvable recurrent network model that links to feed forward networks. By perturbative methods we transform the time-continuous, recurrent dynamics into an effective feed-forward structure of linear and non-linear temporal kernels. The resulting analytical expressions allow us to build optimal time-series classifiers from random reservoir networks. Firstly, this allows us to optimize not only the readout vectors, but also the input projection, demonstrating a strong potential performance gain. Secondly, the analysis exposes how the second order stimulus statistics is a crucial element that interacts with the non-linearity of the dynamics and boosts performance.

1 Introduction

Trained neural networks today form an integral component of data science. Widely used approaches comprise deep neural networks (LeCun, 2015) that typically employ time-independent mappings by hierarchical structures with mostly feed-forward connections. In contrast, recurrent neural networks, which follow more closely their biological counterparts in the brain, have units with intrinsic temporal dynamics that allow natural processing of time-dependent stimuli. The interplay of recurrence and non-linearity in such networks renders their analysis challenging. There is large interest in understanding the basis for their computational abilities. Reservoir computing, as originally introduced via Echo State Networks (Jaeger, 2001) and Liquid State Machines (Maass et al., 2002), is one approach that takes recurrence of connections and temporal dynamics into account. Signals are here mapped into a high dimensional space spanned by a large number of typically randomly connected neurons, on which a linear readout is trained. The network thereby acts like a kernel in a support vector machine (Vapnik, 1998; Cortes and Vapnik, 1995). The training can be combined with a feedback of the readout signal to effectively modify also the recurrent connections (Sussillo and Abbott, 2009; DePasquale et al., 2018). The gradient of an arbitrary loss function for these models can be computed memory efficiently via ordinary differential equations (Chen et al., 2018). Although recurrent models lately have become more and more complex (Hochreiter and Schmidhuber, 1997; Cho et al., 2014; Collins et al., 2016), they remain highly similar to simple reservoirs in terms of the

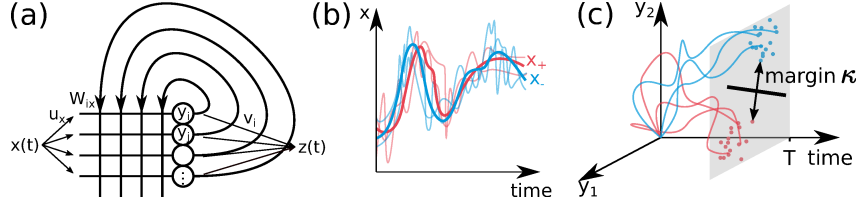


Figure 1: *Binary classification with recurrent dynamics.* (a) A neural network with random connectivity W is stimulated with an input $x(t)$ via an input vector u (left). A linear readout with weights v transforms the high dimensional state into a scalar quantity $z(t)$. (b) Time course of sample stimuli (colored thin curves) from two different classes (red, blue; thick curves: class average). In this example, classes differ mainly in fluctuations. (c) Responses of the network follow high-dimensional trajectories (colored curves, only two dimensions y_1, y_2 shown for conceptual clarity). At readout time T , the samples form clouds of states, indicated by points in the readout time plane. Classification places a decision plane between the classes. The margin κ is the smallest distance between the states and the plane.

learned neural representations (Maheswaranathan et al., 2019). Furthermore, it has been extensively studied how the performance of the reservoir depends on the properties of the recurrent connectivity; the edge of chaos has been found as a global indicator of good computational properties (Bertschinger et al., 2005; Toyozumi and Abbott, 2011). However, the interplay of recurrence and non-linearities may, depending on the statistical features of the input data, offer optimal settings that are not described by such global parameters alone.

We here set out to systematically analyze the kernel properties of recurrent time-continuous networks in a binary time series classification task. We show how the high-dimensional and non-linear transformation implemented by the network can be used to selectively extract differences in the statistics between a pair of input classes. To this end, we analyze the mapping between the input data distribution and the shape and linear separation of the resulting network states, which uniquely determine the optimal readout projection. In state-of-the-art reservoir computing, the projection of the stimuli into the network is mostly carried out with random weights. To the contrary, we here show that the classification performance crucially depends on the input projection; random projections consistently lead to significantly sub-optimal performance, whereas an optimal input projection exploits the mode landscape of the reservoir to obtain an advantageous configuration of the resulting distribution of network states. We derive a method to jointly optimize both projections in a system of linear units and generalize these results to non-linear networks. To this end, we employ a perturbative approach that transforms the non-linear recurrent network into an effective feed-forward structure. The analytical expressions expose how the network dynamics separates a priori linearly non-separable time-series. We find that even weak non-linearities can significantly boost the separability of network states if the linear separability of the stimuli is low.

2 Setup

We consider a reservoir model shown in figure 1(a): A time-dependent input function $x(t)$ is projected into the N -dimensional neuron space with input projection $u \in \mathbb{R}^N$. This signal reverberates in the network through continuous interactions via recurrent connections $W \in \mathbb{R}^{N \times N}$ as well as sustained external stimulation, leading to a neural trajectory $y(t) \in \mathbb{R}^N$ that is described by the first-order differential equation (Sompolinsky et al., 1988)

$$(\tau \partial_t + 1) y_i(t) = \sum_j W_{ij} \phi(y_j(t)) + u_i x(t), \quad (1)$$

where ϕ is the (non-linear) gain function of the neurons. The network activity is read out linearly by the one-dimensional projection $z(t) = v^T y(t)$, obtained with readout vector $v \in \mathbb{R}^N$. We here consider fixed realizations of i.i.d. weights $W_{ij} \sim \mathcal{N}(0, \frac{q^2}{N})$ denoting the connections from neurons j to neurons i and aim towards a joint optimization of input and readout projections u and v , respectively. In general, the existence of optimal projection vectors allows one to first define and second study the performance of the recurrent reservoir itself. Thus, common methods for optimizing recurrent

connectivity can be combined with our algorithm to study and improve the kernel properties of a reservoir network, eliminating variability of performance caused by sub-optimal input and readout projections.

Consider inputs from two classes $+$, $-$ defined by their underlying statistics, for example their mean trajectories and fluctuations, as shown in figure 1(b). The network transforms the differences across classes into distinct sets of network states $y_{\pm}(t)$, which form extended clouds in state space due to intra-class variability (figure 1(c)). For classification, the network space is divided by a hyperplane into one region for each class. Position and orientation of this plane are modified by the training algorithm of the readout projection v , the hyperplane's normal vector. The margin, the distance between the plane and the sample state closest to it, is hereby a typical optimization objective (Vapnik, 1998; Cortes and Vapnik, 1995).

3 Linear Networks

To introduce the concepts, we first investigate the benefits of optimized input projections for linear reservoirs, where $\phi(y) = y$ in equation (1). The linear equation of motion has the Green's function (Risken, 1996)

$$G^{(1)}(t, t') = H(t - t') \frac{1}{\tau} \exp \left[-(\mathbb{I} - W) \frac{t - t'}{\tau} \right], \quad (2)$$

where H is the Heaviside function. The state of neuron i at time point t is then given by

$$y_i(t) = \sum_p \int_{-\infty}^{\infty} dt' G_{ip}^{(1)}(t, t') u_p x(t'). \quad (3)$$

The margin between classes of stimuli with class labels $\zeta_{\nu} \in \pm 1$

$$\kappa(u, v) = \min_{\nu} (\zeta_{\nu} v^T y^{u, \nu}), \quad (4)$$

where v has unit length, constitutes a measure to be optimized to increase generalization performance. We here denote by $y^{u, \nu}$ the network response to stimulus x^{ν} projected via input vector u , and we assumed that the separating hyperplane passes through the origin. This choice is adequate for the stimulus set employed below. Shifting the plane off the origin can be accounted for by incorporation of a threshold. The margin κ depends on both the input projection u and the readout v . For a given set of training data, its maximum is uniquely defined by the support vector machine algorithm (Vapnik, 1998; Cortes and Vapnik, 1995). For the joint optimization of input and readout projections we pursue here, we use this objective as the basis to derive analytically tractable approximations.

For generality of the optimal projection vectors and analytical insight, it is advisable to replace the minimum function in equation (4) by a differentiable approximation, leading us to a soft margin which takes into account not only the outliers, but all points weighted by their distance to the classification plane. This has the advantage to tolerate some outliers if this improves the distance for the majority of samples that are closer to the plane. Here we use a soft margin of the form (Lange et al., 2014)

$$\kappa_{\eta}(u, v) = -\frac{1}{\eta} \ln \left[\sum_{\nu} \exp(-\eta \zeta_{\nu} v^T y^{u, \nu}) \right]. \quad (5)$$

The control parameter η regulates the importance of distances of states close to and far from the separating hyperplane. For $\eta \rightarrow \infty$, we recover the margin $\kappa = \lim_{\eta \rightarrow \infty} \kappa_{\eta}$. For finite η , the soft margin becomes less sensitive to the exact realizations of the network states than the margin κ (equation (4)). We show in the supplementary material (section A.1) by Hölder's inequality that equation (5) is in fact concave in v ; it thus possesses a unique maximum in v . As we presume a large number of samples representing the distribution of stimuli, we can express the sum by an expectation value with respect to the underlying probability distribution of $\zeta_{\nu} y^{u, \nu}$,

$$\kappa_{\eta}(u, v) \rightarrow -\frac{1}{\eta} \ln \langle \exp(-\eta \zeta_{\nu} v^T y^{u, \nu}) \rangle,$$

where we neglected an inconsequential offset. The soft margin κ_{η} has now the form of a scaled cumulant generating function (Gardiner, 1985; Touchette, 2009); its Taylor expansion until the second cumulant of $\zeta_{\nu} y^{u, \nu}$ thus reads

$$\kappa_{\eta}(u, v) \approx v^T M u - \frac{1}{2} \eta v^T \Sigma u v, \quad (6)$$

where $M_i^u := \langle \zeta_\nu y_i^{u,\nu} \rangle$ is the average separation vector between the center of the clouds and the decision plane and $\Sigma_{ij}^u := \langle (\zeta_\nu y_i^{u,\nu}) (\zeta_\nu y_j^{u,\nu}) \rangle - M_i^u M_j^u$ the covariance matrix. The two terms have counteracting effects on the soft margin. The decomposition of the soft margin into cumulants of labeled network states shows a suppression of cumulants of order k by a factor $\frac{1}{k!}$. It is also geometrically plausible that lower order cumulants are more important than higher orders; they describe the rough shape of the state clouds. Stopping after second order amounts to a Gaussian approximation of the state clouds. Alternatively, one can regard equation (6) as classification by linear discriminant analysis if the two sample classes are of equal size (Minasny, 2009); when further assuming Gaussianity and equal variance of the two classes, this is identical to Fisher linear discriminant analysis. From now on, the term soft margin will refer to equation (6).

Since a linear gain function $\phi(y) = y$ imposes a linear relationship between network inputs and outputs (equation (3)), each cumulant of the network state depends only on the corresponding cumulant of the stimulus. Separation between the classes is thus linearly related to the difference between mean stimuli of the two classes. In contrast, in non-linear networks higher order cumulants also contribute to the separation between the classes.

Optimization of the soft margin can be done for arbitrary input signals. However, since equation (6) only depends on the mean and covariance of network outputs, it is sufficient for linear networks to regard stimuli as coming from a Gaussian distribution. As an example, in the following the stimuli are furthermore taken as step-wise constant, accounting for a finite temporal resolution Δt that would typically appear in a practical application. We therefore replace the dependence on the stimulus time t' in the Green's function by the index n , where $t_n = n \Delta t$, defining $G_{ipn}^{(1)}(t) := \int_{t_n}^{t_{n+1}} G_{ip}^{(1)}(t, t') dt'$. Without loss of generality we can assume the distribution of stimuli to be of the form

$$x^\pm \propto \mathcal{N}(\pm\mu, \psi \pm \chi), \quad (7)$$

where $\mu \in \mathbb{R}^{T/\Delta t}$ and $\psi, \chi \in \mathbb{R}^{T/\Delta t \times T/\Delta t}$. A potential offset in the mean could be absorbed by a corresponding threshold in equations (4) - (6) and different covariances C^\pm are included by setting $\psi := \frac{1}{2}(C^+ + C^-)$ and $\chi := \frac{1}{2}(C^+ - C^-)$. It is straightforward to then compute the average separation at time T

$$M_i^u = \sum_{p,n} G_{ipn}^{(1)}(T) u_p \mu_n$$

and the covariance

$$\Sigma_{ij}^u = \sum_{n,m,p,q} G_{ipn}^{(1)}(T) G_{jqm}^{(1)}(T) u_p u_q \psi_{nm}.$$

The soft margin (equation (6)) is thus quadratic in both the input projection u and the readout vector v and therefore simple to optimize with respect to either of them. Hereby, we require both projection vectors to be normalized. For the readout, this ensures a meaningful calculation of the margin. For the input projection, this fixes the amplitude of the driving signal (cf. section 4 and supplementary material (section A)). A constrained optimization follows with the method of Lagrange multipliers by computing the stationary points of

$$\mathcal{L}(u, v) := \kappa_\eta(u, v) + \lambda_u (\|u\|^2 - 1) + \lambda_v (\|v\|^2 - 1) \quad (8)$$

with $\lambda_{u/v} < 0$ (see supplementary material, section A.3). This equation can be maximized by alternating fixed-point iteration. In case $\mu = 0$, the soft margin is a quadratic form and finding the optimal projection vectors reduces to an eigenvalue problem. A detailed description of the optimization process is given in the supplementary material, section A.

Figure 2 shows the increase in soft margin by optimizing the input projection u in the linear reservoir. Inspecting the time span just prior to the readout time point T exposes the high sensitivity of the soft margin to the readout time point (Figure 2a). The global optimum may thus be reached at some intermediate time point, prior to the end of the stimulus; it is possible that later steps of the stimuli counteract the separation or disturb the favorable orientation of the state clouds. On average over many sets of stimuli, however, the soft margin increases towards late readout times (Figure 2b), indicating that the reverberating activity of the network can effectively be used to accumulate evidence. Networks closer to instability with longer time constants or a time-integrated readout may therefore be beneficial for the performance, particularly in the example shown in section 5. Qualitatively, the dominance of the more recent past of the stimulus, however, prevails. An average over stimuli of the

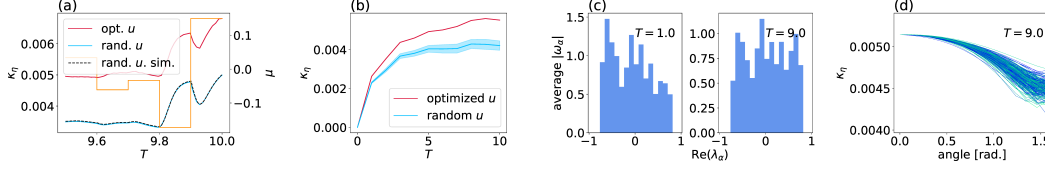


Figure 2: *Optimization of the input and readout projections in a reservoir of linear units.* (a) Random network with $N = 100$ neurons, $\tau = 0.25$ and fixed connectivity W ($W_{ij} \sim \mathcal{N}(0, \frac{g^2}{N})$, $g = 0.9$) is stimulated by step-wise constant stimuli with a mean separation of $\mu = \frac{1}{2}(x_+(t) - x_-(t))$ (orange, right scale). The soft margin (left scale) when stimulated with a random input projection, but readout vector optimized according to equation (6) (blue: analytical solution (equation (3)), black dashed: simulation result (Gewaltig and Diesmann, 2007)) with $\eta = 10$ is shown alongside the combined optimization using 30 optimization steps of input and readout projection at readout time T (red). (b) The same network is stimulated with 250 random stepwise constant signals with optimized (red) and 250 random (blue) input projections each. The corresponding readout projection is chosen optimally in either case. The soft margins, averaged over stimuli, are shown for both cases. Colored area marks the standard deviations of κ_η with respect to random input projections averaged over stimuli. (c) At readout times $T = 1$ and $T = 9$, the optimal input projections of the samples used in (b) are decomposed into eigenmodes of the reservoir. Histograms show the average absolute weight ω_α of the modes corresponding to an eigenvalue λ_α ; real part determines the time constant τ_α of the mode. (d) Soft margin for varying input projection u that has the given angle on the abscissa to the optimal direction u^* at readout time $T = 9$; u is oriented within a randomly chosen hyperplane.

decomposition $\omega_\alpha = w_\alpha^T u$ of the optimal input projections into eigenmodes w_α of the connectivity, $w_\alpha^T W = \lambda_\alpha w_\alpha^T$, is shown in Figure 2(c). The information projected on each mode thereby decays exponentially with time constant $\tau_\alpha = \tau (1 - \text{Re}(\lambda_\alpha))^{-1}$. Pronounced contributions of modes with short time constants at both early and late readout times emphasize the importance of the recent past of the stimulus for classification. Perturbing the input projection u into random directions shows that the optimal direction is sharply defined (Figure 2(d)).

4 Non-linear Networks

Classification by a linear system fails when stimuli become linearly inseparable, because the mapping of the stimulus into the state space of the network can only perform a linear transformation. The introduction of a non-linear activation function qualitatively changes this result. Interpreting the processing in the network as a kernel functional, the space it belongs to is thus extended: to leading order in a perturbative expansion, the mapping changes from a linear functional to a quadratic functional; that is, a functional in which pairs of time points of the input signal contribute to the network output at any given point in time. These non-linear interactions render the system sensitive to class-specific characteristics also in higher order cumulants. The soft margin therefore profits from more contributions to the distance M and covariance Σ of the state clouds. The approach therefore elucidates which statistical features of the input data can be used by the network, thus opening a door to link and compare reservoir computing to feature-based approaches of classification.

We focus on the case where the neural gain function is explored only in a confined area around a working point, where the non-linearity remains small, so we expand the gain function as $\phi(y) \simeq y + \alpha y^2 + \mathcal{O}(y^3)$ with a small, positive parameter $0 \leq \alpha \ll 1$, and a small or vanishing initial condition for y . In the context of biological neural networks, the gain function represents the non-linearity experienced by a single synaptic input on the background noise caused by the other inputs. It is formally obtained by a Gram-Chalier expansion; an expansion in the non-Gaussian cumulants of a nearly Gaussian distributed input. (Dahmen et al., 2016) and (Farkhooi and Stannat, 2017) have explored such expansions for binary networks and found that even the linear order provides a good approximation of the recurrent dynamics, as soon as the number of inputs per neuron is on the order of 50 – 100. For conceptual clarity, we here focus on the simpler case of a rate network, but more elaborate methods are also conceivable. The corresponding Green’s function for the network can be

derived from a perturbation expansion of the corresponding network dynamics in orders of α as

$$y(t) = y^{(0)}(t) + \alpha y^{(1)}(t) + \mathcal{O}(\alpha^2). \quad (9)$$

Inserting the ansatz (equation (9)) into equation (1) separates the solution into different orders of α . The zeroth order,

$$(\tau \partial_t + 1) y_i^{(0)}(t) - \sum_j W_{ij} y_j^{(0)}(t) = u_i x(t) + \mathcal{O}(\alpha), \quad (10)$$

recovers the linear system, solved by equation (3). Corrections to the dynamics can be found in higher orders in α . With use of equation (10), the differential equation (equation (1)) with terms up to first order in α simplifies as

$$(\tau \partial_t + 1) y_i^{(1)}(t) - \sum_j W_{ij} y_j^{(1)}(t) = \sum_j W_{ij} (y_j^{(0)}(t))^2. \quad (11)$$

The first non-linear correction to the linear dynamics obeys the same differential equation as the linear one, with the linear solution entering the inhomogeneity in the place of $u_i x(t)$. Thus, $y^{(1)}$ follows with the Green's function $G^{(1)}$ (equation (2)) and equation (11) as

$$\begin{aligned} \alpha y_i^{(1)}(t) &= \alpha \sum_{i',j} \int_{-\infty}^{\infty} dt' G_{ii'}^{(1)}(t, t') W_{i'j} [y_j^{(0)}(t')]^2 \\ &=: \sum_{p,q} \int_{-\infty}^{\infty} ds \int_{-\infty}^{\infty} ds' G_{ipq}^{(2)}(t, s, s') u_p u_q x(s) x(s'), \end{aligned} \quad (12)$$

where we defined the second order Green's function $G^{(2)}$ and $y_j^{(0)}(t')$ is the zeroth order solution of equation (10) given by equation (3). At this order, the reservoir thus maps the input by a bi-linear functional kernel to the output. Concerning the validity of the approximation, it must be noted that, whereas the solution of the linear system remains well-defined also in the linearly unstable regime, the perturbative solution of the non-linear system built thereof (equations (9) - (12)) in that case suffers from exponentially growing modes. Therefore, we do not consider chaotic networks in our analysis, restricting the variance of connectivity weights to $g < 1$.

Figure 3(a) shows that the first order correction in α approximates the dynamics of the full system quite well. For small α , the network is linearly stable: the eigenvalues $\tilde{\lambda}$ of the linearized connectivity (see supplementary material, section A.2) $\tilde{W}_{ij} = W_{ij}(1 + 2\alpha y_j(t))$ fulfill $\max(\text{Re}(\tilde{\lambda})) < 1$ (Figure 3a, right inset). Consequently, the difference between the linear and non-linear system is not large. Yet, we will show that the non-linearity has a considerable impact on the separability of inputs where the linear theory alone fails to separate the stimuli.

Given the Green's functions $G^{(1)}$ and $G^{(2)}$, the expected distance and covariance required for evaluation of the soft margin in equation (6) can be computed using

$$\zeta_\nu y_i^{u,\nu} = \sum_{p,n} G_{ipn}^{(1)}(T) u_p \zeta_\nu x_n^\nu + \sum_{p,q,m,n} G_{ipqnm}^{(2)}(T) u_p u_q \zeta_\nu x_n^\nu x_m^\nu. \quad (13)$$

The distance M between the state clouds thereby receives $\mathcal{O}(\alpha)$ contributions from the first two cumulants of the stimuli, whereas the covariance Σ receives corrections up to $\mathcal{O}(\alpha^2)$ from stimulus cumulants up to fourth order. Although $\mathcal{O}(\alpha^2)$ corrections to Σ form only a small modification to the covariance that is otherwise determined up to $\mathcal{O}(\alpha)$, this term is essential to guarantee its positive definiteness. A consistent calculation of network state cumulants is therefore required for a stable optimization algorithm. It is easy to show that all orders in α of both M and Σ are affected by Gaussian distributed stimuli. The latter is therefore the minimal example to expose cumulant-mixing based on non-linearities. Contributions from higher order cumulants of stimuli would not show qualitatively different effects.

Equation (8) can thus be expressed with help of equation (13). As in the linear case it is bi-linear in v , but due to Σ it now contains terms with third and fourth power in u . By the bi-linearity in v , the readout projection is determined as in the linear case, only with additional contributions to the covariance matrix and distance vector. The optimization of the input projection, by contrast, is more challenging. The higher powers of u impede a direct solution. In our analysis, the most

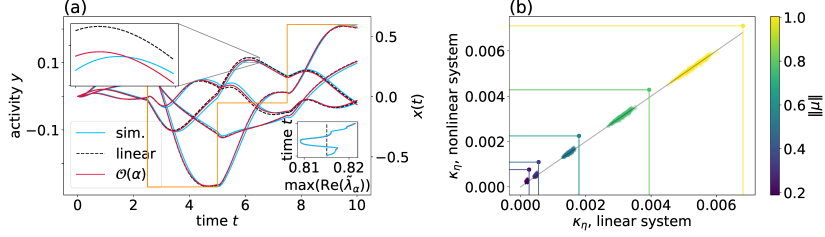


Figure 3: *Responses and soft margins in a network with small non-linearity α .* (a) First order approximation $\mathcal{O}(\alpha)$ of the dynamics (red) and linear response (black dashed). Simulation shown in blue. Left inset shows a zoom in, right inset shows time evolution of $\max_{\alpha}(\text{Re}(\tilde{\lambda}_{\alpha}))$ for simulation (blue) and $\mathcal{O}(\alpha)$ approximation (red) of the nonlinear reservoir together with $\max_{\alpha}(\text{Re}(\lambda_{\alpha}))$ (black dashed) of the linear reservoir. (b) Soft margins κ_{η} for random (stars) and optimized input projections v with respect to equation (8). Linear system on x-axis, non-linear system on y-axis. Vertical and horizontal colored lines at position of optimized solution provided as a guide. Gray line is the angle bisector. Colors indicate $\|\mu\|$, the strength of linear separability of the underlying stimulus distribution, where $\|\mu\| \in \{0.19, 0.30, 0.52, 0.76, 1.0\}$ from violet to yellow. Both ψ and χ are held constant with eigenvalues of $\psi \pm \chi$ in the range $[0.3, 2.2]$. Same parameters as in figure 2, but with $\alpha = 0.05$ for the non-linear system.

reliable optimization scheme proved to be searching for a direct solution to $\partial_u \mathcal{L}(u, v) = 0$ given by equation (8) with an appropriate initial guess. More details and pseudocode can be found in the supplementary material (section A.3).

How much the choice of the input projection affects the soft margin can be observed in figure 3(b). The input and readout projections are optimized separately for a linear and a non-linear network; they take on different optimal values for the two reservoirs. A benefit of optimizing the input projection in the linear reservoir only occurs for increasing strength in the mean class difference μ . For small μ , the optimal direction is dominated by the one that minimizes the effect of the noise, while for larger μ , the stimulus direction aligns such as to maximize the mean separation of the output of the network. The situation is clearly different in the non-linear reservoir even for the weak non-linearity considered here: At low linear separabilities of inputs, the optimization of the input projection in the non-linear reservoir yields a strong relative improvement in separability of outputs, indicated by the soft margin. For linearly well separable classes the relative improvement with respect to the linear reservoir shrinks, while the absolute improvement stays rather constant. Close to the information theoretic optimum of perfectly separable classes considered in the dataset application in section 5, the benefit of non-linearities becomes negligible. The superior performance of the weakly non-linear system with respect to the linear system vanishes for all input separabilities if input projections are not optimized: For random input projections, the performance in the non-linear reservoir is on average only slightly better, and sometimes even worse, than in the linear reservoir. The random input projections accumulate along the identity line in figure 3(b), with a center of mass slightly in the upper area.

In summary, while the weak non-linear corrections to the linear dynamics as used here do not exploit the full computational power non-linearities can exert, the presented routine allows us to inspect the potential of this framework that is not apparent in classical reservoir computing with random input projections.

5 Application to ECG5000 dataset

We conclude the analysis with an application to a univariate temporal classification dataset. This serves as a proof-of-concept to demonstrate the effects of the optimization on a real-world problem and can be regarded as a check that real data do not generally contain structural obstacles that were not covered in the theoretical considerations. To raise the method from the proof-of-concept level, the performance should be systematically checked on a broader set of problems as done for state

Table 1: *Quality measures for the application of the optimization scheme to ECG5000.* Soft margin κ_η (left) and accuracy (right) for optimized and 50 random input projections, averaged over 20 different network realizations.

	κ_η , linear	κ_η , non-linear	accuracy, linear	accuracy, non-linear
random u	0.182 ± 0.015	0.183 ± 0.015	$(91.7 \pm 0.6) \%$	$(91.7 \pm 0.7) \%$
optimized u	0.383 ± 0.026	0.384 ± 0.026	$(97.3 \pm 0.4) \%$	$(97.3 \pm 0.4) \%$

of the art time series classifiers (Bagnall et al., 2017; Wang et al., 2017), which we leave for future work.

We here restrict the preprocessing of the data to a minimum. In this spirit, also the free parameters η and τ are chosen appropriately, but not optimally. The focus lies solely on a comparison between random and optimized input projections. This comparison is based on the classification soft margin and accuracy in a fixed reservoir configuration. We can then observe the effect of the optimization routine on the separation and covariance of the state clouds.

The examined dataset is ECG5000, which is publicly available at the UCR Time Series Classification archive (Chen et al., 2015), containing 5000 electrocardiograms of single heartbeat recordings. The classes separate between five categories of healthy and diseased heartbeats. For a binary classification, we use only samples from the two largest classes, so that we obtained a training set consisting of 354 samples and a testing set of 4332 samples. All stimuli were shifted and scaled to provide classes with means $\pm\mu$ with $\|\mu\| = 1$; higher order cumulants changed accordingly. This scaling of inputs is only performed for conceptual clarity, allowing identical network parameters as in the previous task. Likewise, one could adapt the value of α according to the stimulus strength. Furthermore, for maximal performance, a trained threshold can replace the centering of data. As a measure of linear separability, we relate the difference of the class means to the covariance in the direction of separation. This yields a ratio $\|\mu\|^2/\sqrt{\mu^T \psi \mu} = 2.6$, which is much higher than for the artificial stimuli analyzed in figure 3, where the corresponding measure ranges between 0.19 and 0.98.

All results presented here use the same parameters as in figure 2 and figure 3.

The summary of the results in table 1, which contains averaged results over 20 different initializations of the recurrent connectivity, makes evident that a maximized soft margin is accompanied by increased accuracies. The optimized input projections outperformed all randomly chosen ones both with respect to soft margin and accuracy. Because of the close to perfect linear separability of the data, the increase of soft margins and accuracies from the linear to the non-linear reservoir is very small (see supplementary material, section ??). These results are as theoretically expected from figure 3(b) for linearly well separable data. An application to a broader set of real world data would be required to quantify the performance increase in terms of accuracy also in the case of linearly less separable stimuli.

A visualization of the optimization in figure 4 shows the increase of distance between the classes before and after optimization (a, b), gradually increasing with the optimization step (c). The projections being optimized for $T = 10$, the two classes become distinguishable only shortly before this readout time point (d). The variance along the readout direction $\frac{\eta}{2}v^T \Sigma^u v$ is hereby rather constant, while the main deviations occur due to the separation. Increasing η can be used to enforce smaller dispersion of the state clouds (see supplementary material, section ??). The enlarged range in between the class centers with low probability density for network states of either class facilitates a better generalization to unknown data.

6 Discussion

We present an analytical approach of unrolling recurrent non-linear networks by use of a perturbative expansion. The conceptual insight of this step lies in a simplification of the reverberating neuronal dynamics into an effective feed-forward structure. This approach, which involves the first and second order Green’s function of the system, extends naturally from linear networks to non-linear ones. The reformulation of the classification margin as a partly concave soft margin, which has a similar form as a free energy, facilitates the derivation of closed-form expressions to be maximized. The joint optimization of stimulus projection and readout vector leads to a significant increase in

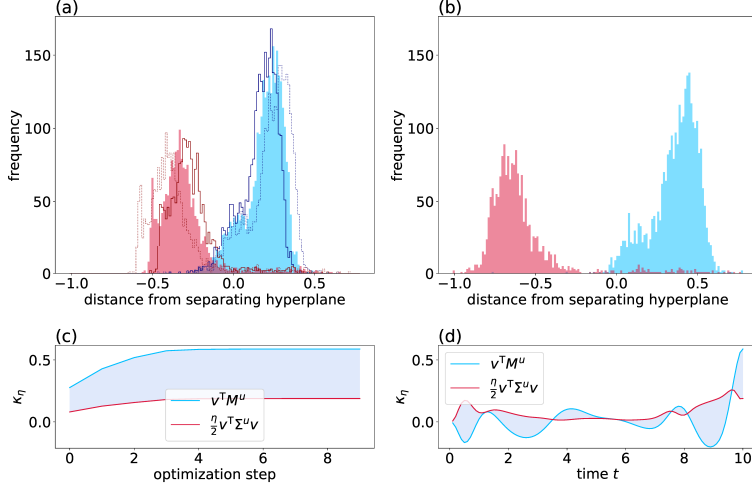


Figure 4: *Network state distribution for random and optimal input projection.* (a) Random input projections: Colored histogram shows the network state distribution for both classes in direction of the separating hyperplane’s normal vector (average over 50 input projections). Light and dark outlined histograms correspond to the input vectors with the best and worst accuracies among the drawn samples, respectively. All network states are based on $\mathcal{O}(\alpha)$ -predictions of the dynamics. (b) Optimized input projection: Histogram of the network state distribution (based on the simulated responses). (c) Evolution of distance and covariance contribution to the soft margin κ_η over the first 10 optimization steps at readout time. Height of the shaded area corresponds to the resulting κ_η , illustrating the difference between the two terms in equation (6). (d) Evolution of distance and covariance contribution to κ_η over simulation time for optimized input vector u . Height of the shaded area corresponds to the soft margin (negative where covariance contribution (red) exceeds distance contribution (blue) and positive otherwise). Same network and parameters as in figure 3.

classification performance by tuning the network state distribution towards a trade-off between low variability along the direction of separation and high absolute separation. This increase of separability is in particular observable even in only weakly non-linear networks when the linear separability of the stimuli is low. The effect can be fully explained by the second order Green’s function that makes the reservoir sensitive to classification features in the second order stimulus statistics. We find that the effect of higher statistical orders of the data are suppressed by powers in the perturbation parameter, the non-linearity of the neuronal dynamics. But also the classification performance of the linearly well separable dataset ECG5000 profits significantly from the optimization. The framework presents a stepping stone towards a systematic understanding of information processing by recurrent random networks.

Acknowledgements

This work was partly supported by European Union Horizon 2020 grant 945539 (Human Brain Project SGA3), the Helmholtz Association Initiative and Networking Fund under project number SO-092 (Advanced Computing Architectures, ACA), BMBF Grant 01IS19077A (Juelich) and the Excellence Initiative of the German federal and state governments (G:(DE-82)EXS-SF-neuroIC002).

Broader impact

The main motivation of this work is to provide conceptual insight. Analytically unrolling recurrent dynamics into a (functional) Taylor series, where coefficients are given by Green’s functions, is a versatile approach that may be used as a general purpose scheme to analyze recurrent networks and to optimize reservoir computing. This expansion reveals how the non-linear interactions and recurrence pick up higher order correlations in the input statistics, quantifying how non-linear networks provide a richer feature space than linear ones. We consider the presented application as a

proof-of-principle for optimized processing of complex time series data. The presented application to health-related data (heartbeat classification) hints at possible societal consequences by providing better diagnostic tools.

References

- Anthony Bagnall, Jason Lines, Aaron Bostrom, James Large, and Eamonn Keogh. The great time series classification bake off: a review and experimental evaluation of recent algorithmic advances. *Data Mining and Knowledge Discovery*, 31(3):606–660, 2017.
- Nils Bertschinger, Thomas Natschläger, and Robert A Legenstein. At the edge of chaos: Real-time computations and self-organized criticality in recurrent neural networks. In *Advances in neural information processing systems*, pages 145–152, 2005.
- Ricky TQ Chen, Yulia Rubanova, Jesse Bettencourt, and David K Duvenaud. Neural ordinary differential equations. In *Advances in neural information processing systems*, pages 6571–6583, 2018.
- Yanping Chen, Eamonn Keogh, Bing Hu, Nurjahan Begum, Anthony Bagnall, Abdullah Mueen, and Gustavo Batista. The ucr time series classification archive. 2015. URL https://www.cs.ucr.edu/%7Eeamonn/time_series_data_2018/.
- Kyunghyun Cho, Bart Van Merriënboer, Caglar Gulcehre, Dzmitry Bahdanau, Fethi Bougares, Holger Schwenk, and Yoshua Bengio. Learning phrase representations using rnn encoder-decoder for statistical machine translation. *arXiv preprint arXiv:1406.1078*, 2014.
- Jasmine Collins, Jascha Sohl-Dickstein, and David Sussillo. Capacity and trainability in recurrent neural networks. *arXiv preprint arXiv:1611.09913*, 2016.
- Corinna Cortes and Vladimir Vapnik. Support-vector networks. *Machine learning*, 20(3):273–297, 1995.
- David Dahmen, Hannah Bos, and Moritz Helias. Correlated fluctuations in strongly coupled binary networks beyond equilibrium. *Physical Review X*, 6(3):031024, 2016.
- Brian DePasquale, Christopher J Cueva, Kanaka Rajan, G Sean Escola, and LF Abbott. full-force: A target-based method for training recurrent networks. *PLoS one*, 13(2), 2018.
- Farzad Farkhooi and Wilhelm Stannat. Complete mean-field theory for dynamics of binary recurrent networks. *Physical review letters*, 119(20):208301, 2017.
- Crispin W. Gardiner. *Handbook of Stochastic Methods for Physics, Chemistry and the Natural Sciences*. Number 13 in Springer Series in Synergetics. Springer-Verlag, Berlin, 2nd edition, 1985. ISBN 3-540-61634-9, 3-540-15607-0.
- Marc-Oliver Gewaltig and Markus Diesmann. NEST (NEural Simulation Tool). *Scholarpedia*, 2(4): 1430, 2007.
- N Goldenfield. Lectures on phase transformations and the renormalization group. *Frontiers in Physics*, 1992.
- Sepp Hochreiter and Jürgen Schmidhuber. Long short-term memory. *Neural computation*, 9(8): 1735–1780, 1997.
- H. Jaeger. The “echo state” approach to analysing and training recurrent neural networks. Technical Report GMD Report 148, German National Research Center for Information Technology, St. Augustin, Germany, 2001.
- Mandy Lange, Dietlind Zühlke, Olaf Holz, Thomas Villmann, and Saxon-Germany Mittweida. Applications of lp-norms and their smooth approximations for gradient based learning vector quantization. In *ESANN*, 2014.
- Yann LeCun. Yoshua bengio, and geoffrey hinton. *Deep learning. nature*, 521(7553):436–444, 2015.

- Wolfgang Maass, Thomas Natschläger, and Henry Markram. Real-time computing without stable states: A new framework for neural computation based on perturbations. *Neural computation*, 14(11):2531–2560, 2002.
- Niru Maheswaranathan, Alex Williams, Matthew Golub, Surya Ganguli, and David Sussillo. Universality and individuality in neural dynamics across large populations of recurrent networks. In *Advances in neural information processing systems*, pages 15629–15641, 2019.
- Budiman Minasny. The elements of statistical learning, trevor hastie, robert tishirani, jerome friedman, (2009), springer series in statistics, isbn 0172-7397, 745 pp, 2009. URL <https://web.stanford.edu/~hastie/Papers/ESLII.pdf>.
- Travis E Oliphant. *A guide to NumPy*, volume 1. Trelgol Publishing USA, 2006.
- H Risken. *The Fokker-Planck Equation*. Springer Verlag Berlin Heidelberg, 1996.
- H. Sompolinsky, A. Crisanti, and H. J. Sommers. Chaos in random neural networks. 61:259–262, Jul 1988. doi: 10.1103/PhysRevLett.61.259. URL <http://link.aps.org/doi/10.1103/PhysRevLett.61.259>.
- David Sussillo and Larry F Abbott. Generating coherent patterns of activity from chaotic neural networks. *Neuron*, 63(4):544–557, 2009.
- Hugo Touchette. The large deviation approach to statistical mechanics. *Physics Reports*, 478(1-3): 1–69, 2009.
- Taro Toyozumi and LF Abbott. Beyond the edge of chaos: Amplification and temporal integration by recurrent networks in the chaotic regime. *Physical Review E*, 84(5):051908, 2011.
- Vladimir Vapnik. The support vector method of function estimation. In *Nonlinear Modeling*, pages 55–85. Springer, 1998.
- Zhiguang Wang, Weizhong Yan, and Tim Oates. Time series classification from scratch with deep neural networks: A strong baseline. In *2017 International joint conference on neural networks (IJCNN)*, pages 1578–1585. IEEE, 2017.

A Supplementary material

A.1 Convexity of the soft-margin

The soft margin κ_η (equation (5)) is concave in v ; this follows directly from the linear appearance of v in the exponent of the exponential function with Hoelder's inequality. Hoelder's inequality states for two non-negative sequences $g_k, h_k \geq 0$ and for $\alpha + \beta = 1$ that

$$\sum_k (g_k)^\alpha (h_k)^\beta \leq \left(\sum_k g_k\right)^\alpha \left(\sum_k h_k\right)^\beta. \quad (14)$$

We here follow a modified version of the argument in (Goldenfield, 1992). It therefore follows for $\alpha + \beta = 1$ that

$$\begin{aligned} \kappa_\eta(u, \alpha v_1 + \beta v_2) &= -\frac{1}{\eta} \ln \sum_{\nu=1}^P \exp\left(\alpha[-\eta \zeta_\nu(v_1^T y^{u,\nu})] + \beta[-\eta \zeta_\nu(v_2^T y^{u,\nu})]\right) \\ &= -\frac{1}{\eta} \ln \sum_{\nu=1}^P \exp\left(-\eta \zeta_\nu(v_1^T y^{u,\nu})\right)^\alpha \exp\left(-\eta \zeta_\nu(v_2^T y^{u,\nu})\right)^\beta \\ &\stackrel{\text{Hoelder}}{\geq} -\frac{1}{\eta} \ln \left[\sum_{\nu=1}^P \exp\left(-\eta \zeta_\nu(v_1^T y^{u,\nu})\right) \right]^\alpha \left[\sum_{\nu=1}^P \exp\left(-\eta \zeta_\nu(v_2^T y^{u,\nu})\right) \right]^\beta \\ &= \alpha \kappa_\eta(u, v_1) + \beta \kappa_\eta(u, v_2). \end{aligned}$$

A.2 Linearized connectivity

The effective connectivity \tilde{W} is obtained from linearizing around the network's time evolution as

$$\begin{aligned} (\tau \partial_t + 1)(y_i(t) + \delta y_i(t)) &= \sum_j W_{ij} ((y_j(t) + \delta y_j(t)) + \alpha (y_j(t) + \delta y_j(t))^2) + u_i x(t) \\ \Rightarrow (\tau \partial_t + 1) \delta y_i(t) &= \sum_j W_{ij} (1 + 2\alpha y_j(t)) \delta y_j(t) + \mathcal{O}(\delta y^2) \end{aligned}$$

and approximating the non-linear system by an equivalent linear one with connectivity $\tilde{W}_{ij} = W_{ij} (1 + 2\alpha y_j(t))$. The evolution of the system becomes unstable when the real part of an eigenvalue $\tilde{\lambda}_\alpha$ of the effective matrix \tilde{W} exceeds 1. The time evolution of $\max_\alpha (\text{Re}(\tilde{\lambda}_\alpha))$ displayed in Figure 3(a) for the full system and the $\mathcal{O}(\alpha)$ approximation assures the stability of the solution and the quality of the approximation.

A.3 Constrained optimization with Lagrange multipliers

We need to optimize equation (8)

$$\mathcal{L}(u, v) := \kappa_\eta(u, v) + \lambda_u (\|u\|^2 - 1) + \lambda_v (\|v\|^2 - 1),$$

where κ_η takes the form of equation (6). Although the mathematical structure of equation (6) is simple, the optimization of the expression may present a few pitfalls. In this section, we describe in detail how to find the projection vectors given the first four moments of the stimuli.

The linear system can be understood as a special case of the non-linear system, where some contributions to the soft margin and its gradients vanish. Therefore, we will distinguish the types of reservoir kernels only where they are relevant.

A.4 Prerequisites

The numerical results of the optimization slightly depend on the value of the control parameter η of the soft margin that has to be fixed. In our examples, with $\eta = 10$ the soft margin showed already very similar extrema as the margin. Smaller values correspond to softer margins. In practice, a good choice of η can be obtained by comparing for different η the optimized readout vector and

accuracies for responses of some reservoir to an arbitrary stimulation. This procedure is fast and reliable since finding the readout vector for some η is only a quadratic problem. Furthermore, an analysis of the time evolution of the soft margin for random input projections can be used as in figure 2(b) to achieve a good estimate of a suitable τ . It can be chosen such that the soft margin for random stimuli just entered a saturating phase, so that there is not much improvement expected. Extended phases of saturation, however, are a sign of forgetting of early parts of the stimuli in the network and should be avoided.

The main procedure then consists of an alternating optimization of the input and readout projections. Thereby, we denote $\mathcal{L}(u|v)$ as the objective function for input optimization, given v , and $\mathcal{L}(v|u)$ analogously. The resulting algorithm (slightly simplified) is given as pseudocode in algorithm 1.

Algorithm 1 Optimization of equation (8) using Lagrange multipliers.

```

1: COMPUTE( $\sum_n G_{ipn}^{(1)} x_n^\nu, \sum_{n,m} G_{ipqnm}^{(2)} x_n^\nu x_m^\nu$ )
2: for set of initial  $u$  do
3:   repeat
4:     procedure OPTIMIZE INPUT( $\mathcal{L}(u|v)$ )
5:       if  $\|\mu\| = 0$  then
6:         OPTIMIZE( $\kappa_\eta \leftarrow \sum_{p,q} u_p u_q (m_{1pq} - \sigma_{0pq})$ )  $\triangleright$  eigenvalue problem
7:       else if  $\kappa_\eta$  far from saturated then
8:         OPTIMIZE( $\kappa_\eta \leftarrow \sum_p u_p m_{0p} + \sum_{p,q} u_p u_q (m_{1pq} - \sigma_{0pq})$ )  $\triangleright$  quadratic problem
9:       else
10:        OPTIMIZE( $\kappa_\eta \leftarrow \sum_p u_p m_{0p} + \sum_{p,q} u_p u_q (m_{1pq} - \sigma_{0pq}) -$ 
 $\sum_{p,q,r} u_p u_q u_r \sigma_{1pqr} - \sum_{p,q,r,s} u_p u_q u_r u_s \sigma_{2pqrs}$ )
11:      end if
12:    end procedure
13:    procedure OPTIMIZE READOUT( $\mathcal{L}(v|u)$ )
14:      if  $\|\mu\| = 0$  and  $\alpha = 0$  then
15:        OPTIMIZE( $\kappa_\eta \leftarrow -\frac{1}{2}\eta v^T (\Sigma_0 + \Sigma_1)v$ )  $\triangleright$  eigenvalue problem
16:      else
17:        OPTIMIZE( $\kappa_\eta \leftarrow v^T (M_0 + M_1) - \frac{1}{2}\eta v^T (\Sigma_0 + \Sigma_1)v$ )  $\triangleright$  quadratic problem
18:      end if
19:    end procedure
20:  until  $\kappa_\eta$  saturated
21: end for

```

A.5 Optimization of the input projection

The determination of the input projection for fixed readout vector is best conducted, depending on the situation, by one of three methods for non-linear kernels and one of two methods for linear ones. The quantities

$$\begin{aligned}
m_{0p} &= \sum_{i,n} G_{ipn}^{(1)} v_i \langle \zeta_\nu x_n^\nu \rangle \\
m_{1pq} &= \sum_{i,n,m} G_{ipqnm}^{(2)} v_i \langle \zeta_\nu x_n^\nu x_m^\nu \rangle \\
\sigma_{0pq} &= \sum_{\substack{i,j \\ n,m}} \frac{1}{2} \eta G_{ipn}^{(1)} G_{jqm}^{(1)} v_i v_j (\langle x_n^\nu x_m^\nu \rangle - \langle \zeta_\nu x_n^\nu \rangle \langle \zeta_\nu x_m^\nu \rangle) \\
\sigma_{1pqr} &= \sum_{\substack{i,j \\ n,m,o}} \frac{1}{2} \eta (G_{ipn}^{(1)} G_{jqrm}^{(2)} + G_{iqrm}^{(2)} G_{jpn}^{(1)}) v_i v_j (\langle x_n^\nu x_m^\nu x_o^\nu \rangle - \langle \zeta_\nu x_n^\nu \rangle \langle \zeta_\nu x_m^\nu x_o^\nu \rangle) \\
\sigma_{2pqrs} &= \sum_{\substack{i,j \\ n,m,o,l}} \frac{1}{2} \eta G_{ipqmn}^{(2)} G_{jrsol}^{(2)} v_i v_j (\langle x_n^\nu x_m^\nu x_o^\nu x_l^\nu \rangle - \langle \zeta_\nu x_n^\nu x_m^\nu \rangle \langle \zeta_\nu x_o^\nu x_l^\nu \rangle),
\end{aligned}$$

where $G^{(2)}$ is the $\mathcal{O}(\alpha)$ correction of the Green's function $G^{(1)}$ for linear kernels and $\mu = \langle \zeta_\nu x_n^\nu \rangle$, $\psi = \langle x_n^\nu x_m^\nu \rangle - \langle \zeta_\nu x_n^\nu \rangle \langle \zeta_\nu x_m^\nu \rangle$ and $\chi = \langle \zeta_\nu x_n^\nu x_m^\nu \rangle$ constitute the cumulants in the notation (equation (7)) used in the main text. This notation is introduced here and in section A.6 for legibility, although a memory-efficient implementation will compute only products of Green's functions with stimuli x^ν (for example, $\mathcal{G}_{ipq\nu}^{(2)} = \sum_{n,m} G_{ipqm}^{(2)} x_n^\nu x_m^\nu$), which then compose the above abbreviations by performing the averages over ν . With these abbreviations, the dependence of the soft margin on the input projection becomes independent of the length of the input and reads

$$\kappa_\eta = \sum_p u_p m_{0p} + \sum_{p,q} u_p u_q m_{1pq} - \sum_{p,q} u_p u_q \sigma_{0pq} - \sum_{p,q,r} u_p u_q u_r \sigma_{1pqr} - \sum_{p,q,r,s} u_p u_q u_r u_s \sigma_{2pqrs}.$$

Preparations for optimization in non-linear systems

In the non-linear case, it is advisable to take a few precautions to reduce computation time and enhance performance. The determination of the optimal input projection u given a fixed readout projection v should in the first few, but at least one, iterations neglect terms of $\mathcal{O}(\alpha)$ and higher in the covariance Σ^u . In these steps, the soft margin is not strictly optimized, but the result still yields a good initial guess for the full problem. The advantage of this procedure is that the computation is much faster and more likely to achieve a solution near the optimum rather than some local extremum. In the first steps, the direction of the projection vector u typically changes rapidly and the quadratic part alone often has a maximum near the optimum of the full soft margin, as the neglected terms are at least $\mathcal{O}(\alpha)$. In the readout optimization, the problem is in general quadratic in case of both linear and non-linear dynamics, so there is no need to make further simplifications.

Furthermore, the soft margin is not necessarily convex in u in the non-linear case and sometimes exhibits plateaus over iteration steps. We therefore recommend to use a small number of initial projection vectors, optimize them over a few steps as described below, and then proceed with the best one after these steps.

Case A.

The simplest case arises if $\|\mu\| = 0$, since then m_0 , σ_1 and σ_2 vanish, if one neglects the $\mathcal{O}(\alpha)$ contributions in the non-linear case as discussed above. For normalized input projections, equation (6) is then maximized by the eigenvector corresponding to the smallest eigenvalue of $\sigma_0 - m_1$.

Case B.

In the general case where $\|\mu\| \neq 0$, it is, as mentioned before, sometimes helpful to ignore the part related to σ_1 and σ_2 of the soft margin in the non-linear case to obtain a good guess of the input projection that maximizes equation (8). Since m_1 , σ_1 and σ_2 vanish when $\alpha = 0$, the same procedure applies in the linear case. The objective then reads

$$\mathcal{L}(u|v) \rightarrow u^T m_0 + u^T m_1 u - u^T \sigma_0 u + \lambda_u (u^T u - 1),$$

so u and λ_u are found using

$$\partial_u \mathcal{L} = 0 \Rightarrow 2(\sigma_0 - m_1 - \lambda_u \mathbb{I})u = m_0, \quad (15)$$

$$\partial_{\lambda_u} \mathcal{L} = 0 \Rightarrow u^T u - 1 = 0. \quad (16)$$

These equations have many solutions, but for a maximum we further require negative definiteness of $\partial_u^2 \mathcal{L}|_{\lambda_u}$. From this condition follows that $\lambda_u < \min\{\sigma \mid \sigma \text{ is eigenvalue of } \sigma_0 - m_1\}$. Then, $\sigma_0 - m_1 - \lambda_u \mathbb{I}$ is symmetric and invertible and, from solving the first condition for u and inserting in the second, we get

$$\frac{1}{4} (m_0^T (\sigma_0 - m_1 - \lambda_u \mathbb{I})^{-1} (\sigma_0 - m_1 - \lambda_u \mathbb{I})^{-1} m_0) = 1. \quad (17)$$

The term on the left hand side is positive, has poles around the eigenvalues of $\sigma_0 - m_1$ and deviates only slightly from 0 for $\lambda_u \ll \min\{\sigma \mid \sigma \text{ is eigenvalue of } \sigma_0 - m_1\}$. A bisection is therefore best suited to determine λ_u and thereby u using equation (15). This also avoids running into an undesirable solution where $\|u\| \rightarrow 0$ and $\lambda_u \rightarrow -\infty$. However, the poles have only a very small width and the determination of eigenvalues and inverse matrices is accompanied by numerical uncertainties.

Therefore, the upper bound on λ_u is found best as the smallest value within a window of a small width ε around the smallest eigenvalue, where the term on the left hand side exceeds one. Although this corresponds to a fine-tuning of the Lagrange parameter λ_u with a sensitive dependence of the left hand term in equation (17) on the exact used eigenvalues, the soft margins corresponding to the obtained solutions remained robust against neglecting near-vanishing, and therefore numerically uncertain, eigenvalues in the summation. Components of the input projection in these directions are neutralized by their eigenvalues in equation (8).

Case C.

If the system is non-linear and a good initial guess for the input projection is available, predefined solvers, such as the `fsolve` function implemented in `numpy` (Oliphant, 2006), typically find good solutions for the Lagrange conditions, which are in this case

$$\begin{aligned} 2(\sigma_{0pq} - m_{1pq} - \lambda_u \mathbb{I}_{pq})u_q + (\sigma_{1pqr} + \sigma_{1qrp} + \sigma_{1rpq})u_q u_r \\ + (\sigma_{2pqr} + \sigma_{2qrs} + \sigma_{2rsp} + \sigma_{2spqr})u_q u_r u_s = m_{0p}, \\ u^T u = 1. \end{aligned}$$

The first guess should be the solution from the previous iteration step. Only if the soft margin reduces by the found solution, a new guess should be computed neglecting σ_1 and σ_2 . For this comparison, it is important to make sure the projection vectors are properly normalized. Although this is ensured by the Lagrange condition, the actual lengths of the returned vectors slightly deviate from one because of the fine-tuning of the Lagrange parameters. If the soft margin found near that solution still decreases, we decided to use the new solution anyway as a restart-point. The readout vector optimization then improves the soft margin again.

A.6 Optimization of the readout projection

The optimization of the readout projection is structurally the same as for the input projection, only the objective function is in general bi-linear in v . The abbreviations used here are

$$\begin{aligned} M_{0i} &= \sum_{p,n} G_{ipn}^{(1)} u_p \langle \zeta_\nu x_n^\nu \rangle \\ M_{1i} &= \sum_{\substack{p,q, \\ n,m}} G_{ipqnm}^{(2)} u_p u_q \langle \zeta_\nu x_n^\nu x_m^\nu \rangle \\ \Sigma_{0ij} &= \sum_{\substack{p,q, \\ n,m}} G_{ipn}^{(1)} G_{jqm}^{(1)} u_p u_q (\langle x_n^\nu x_m^\nu \rangle - \langle \zeta_\nu x_n^\nu \rangle \langle \zeta_\nu x_m^\nu \rangle) \\ \Sigma_{1ij} &= \sum_{\substack{p,q,r, \\ n,m,o}} (G_{ipn}^{(1)} G_{jqrm}^{(2)} + G_{iqrm}^{(2)} G_{jpn}^{(1)}) u_p u_q u_r (\langle x_n^\nu x_m^\nu x_o^\nu \rangle - \langle \zeta_\nu x_n^\nu \rangle \langle \zeta_\nu x_m^\nu x_o^\nu \rangle) \\ &+ \sum_{\substack{p,q,r,s, \\ n,m,o,l}} G_{ipqmn}^{(2)} G_{jrsol}^{(2)} u_p u_q u_r u_s (\langle x_n^\nu x_m^\nu x_o^\nu x_l^\nu \rangle - \langle \zeta_\nu x_n^\nu x_m^\nu \rangle \langle \zeta_\nu x_o^\nu x_l^\nu \rangle). \end{aligned}$$

The objective function to maximize is then

$$\mathcal{L}(v|u) \rightarrow v^T (M_0 + M_1) - \frac{1}{2} \eta v^T (\Sigma_0 + \Sigma_1) v + \lambda_v (v^T v - 1).$$

Only if the system is linear and the mean stimulus difference μ is vanishing, this becomes an eigenvalue problem and the optimal readout vector v is the eigenvector corresponding to the smallest eigenvalue of Σ_0 (compare case A). Otherwise, the Lagrange parameter follows from a bisection using the conditions

$$\partial_v \mathcal{L} = 0 \Rightarrow (\eta(\Sigma_0 + \Sigma_1) - 2\lambda_v \mathbb{I})v = M_0 + M_1, \quad (18)$$

$$\partial_{\lambda_v} \mathcal{L} = 0 \Rightarrow v^T v - 1 = 0. \quad (19)$$

From negative definiteness, $\lambda_v < \frac{1}{2} \min\{\sigma \mid \sigma \text{ is eigenvalue of } \eta(\Sigma_0 + \Sigma_1)\}$ follows as upper bound on λ_v (compare case B).